The shear modulus and the phase diagram for two-dimensional Wigner electron crystals



1991 J. Phys.: Condens. Matter 3 3493

(http://iopscience.iop.org/0953-8984/3/20/010)

J. Phys.: Condens. Matter 3 (1991) 3493–3503. Printed in the UK

# The shear modulus and the phase diagram for two-dimensional Wigner electron crystals

M J Lea† and N H March‡

† Department of Physics, Royal Holloway and Bedford New College, University of London, Egham Hill, Surrey TW20 0EX, UK

‡ Theoretical Chemistry Department, University of Oxford, 5 South Parks Road, Oxford OX1 3UB, UK

Received 31 December 1990, in final form 20 February 1991

**Abstract.** Defect energies in two- and three-dimensional classical crystals correlate with the shear modulus $\mu$; in turn this relates the melting temperature $T_m$ intimately to $\mu$. Thus, a model is first proposed for the shear modulus for two-dimensional Wigner crystals. The melting temperature is then determined from the Kosterlitz–Thouless melting criterion or from an anharmonic instability inherent in the model. The relative positions of these transitions depend on the model parameters used. The calculation is generalized to include (a) zero-point motion which is dominant in the quantum limit and (b) the effect of a magnetic field. For the high field case, this modelling allows $T_m$ to be plotted versus the Landau-level filling factor $\nu$. The predictions of the model are thereby brought into contact with the experiments of Andrei *et al* and Glattli *et al* which have been interpreted as evidence for a magnetically induced Wigner solid (MIWS) in the electron assembly in a GaAs/AlGaAs heterojunction in strong magnetic fields. The model exhibits some of the features observed experimentally.

## 1. Introduction

In classical monatomic crystals, correlations have long been known to exist between melting temperature $T_m$, vacancy formation energy $E_v$ and elastic moduli. Some understanding of these empirical correlations has been afforded by (a) statistical mechanical models at elevated temperatures, appropriate say to condensed argon (Bhatia and March 1984) and (b) current models of force fields including many-body contributions in metals like Cu (Johnson 1988, see also March 1989). In case (b), Johnson has stressed that the highest correlation among elastic constants and $E_v$ is via the shear modulus $\mu$. While the above relates to three dimensions, the well-known Kosterlitz–Thouless (1973, 1978) transition in two-dimensional classical crystals is driven by the shear modulus and the thermal unbinding of dislocation pairs.

Here the focus is on 2D Wigner electron crystallization, with and without magnetic fields. In zero magnetic field $B$ there is a large body of work to date: we note in particular two very relevant studies. One is the classical limit of the phonon spectrum, worked out by Bonsall and Maradudin (1977). This provides a first-principles basis for scaling the model calculations made in the present paper for the shear modulus. The second is the quantum Monte Carlo study of Ceperley (1978), in which he calculated the mean

0953-8984/91/203493 + 11 $03.50 

interelectronic separation $r_W$, relative to the Bohr radius, at which the transition from electron liquid to 2D Wigner electron crystal occurs, in the quantal limit at $T = 0$. He found the value $r_W = 33$ which again is a most valuable piece of information in the present modelling. Turning to non-zero magnetic fields, which is in fact the prime motivation for the present study, the magnetic-field-assisted Wigner electron crystallization proposed by Durkan *et al* (1968) has been invoked by Andrei *et al* (1988) and Glattli *et al* (1990) as an explanation of their experiments on 2D electrons. These workers demonstrated the sudden onset of a new electron-phonon mode at low frequencies in the electron assembly in a GaAs/AlGaAs heterojunction in a high magnetic field that they suggested was a fingerprint of the magnetically induced Wigner solid (MIWS). They were thus able to map out the melting curve of the proposed Wigner solid as a function of the Landau-level filling factor $\nu = nh/eB$. Once such a plot was made there remained only a rather weak residual dependence on the carrier density, $n$, related to the mean interelectronic separation, $r_0$, by

$$n = (\pi r_0^2)^{-1}. \tag{1.1}$$

While there have been a number of attempts to calculate the melting curve of the Wigner crystal for $B = 0$ (Ferraz *et al* 1978, 1979; Nagara *et al* 1987, see also March 1988), it is only recently that much attention has been focused on melting in the presence of an applied magnetic field (Elliott and Kleppmann 1975, Saitoh 1988, Lea and March 1990). This is therefore one focal point of the present work: to propose a model to predict the melting curve in a magnetic field.

The outline of the paper is then as follows. In section 2, a model calculation is proposed of the shear modulus $\mu$ of a 2D Wigner electron crystal. The idea behind the calculation is motivated by extending the approach of Bonsall and Maradudin (1977), which applied in the limit of complete electron localization. Section 3 is then concerned with self-consistent solutions for three limiting cases of the model: (i) the classical limit, (ii) the quantum limit where zero-point motion dominates and (iii) the high magnetic field regime. The relationship to experiment, both the heterojunction data referred to above for the high magnetic field case and the quantum Monte Carlo result for zero magnetic field, is also given in section 3. A summary is given in section 4, where some proposals for further experiments that would be of interest are put forward.

## 2. Half-width of the electron density profile related to shear modulus

March and Tosi (1985) have considered the effective electron density of a localized Wigner oscillator in a magnetic field $B$ of arbitrary strength. This can be viewed as the Einstein model of a Wigner crystal in an applied magnetic field. As well as for the ground state, the effects of harmonic restoring force, magnetic field and temperature, $T$, still contrive to leave a Gaussian profile for the electron density $\gamma(r)$ at each site, which we shall simply write in the form

$$\gamma(r) = C \exp(-r^2/\lambda^2). \tag{2.1}$$

Here it is evident that the quantity $\lambda$ measures the half-width of the localized electron density profile; this is related to a convenient dimensionless parameter $\sigma$ which we shall take as the root-mean-square shear strain below. It is clear that these two quantities are intimately linked. For zero-point Debye shear waves the mean-square shear strain, or

differential shear displacement, $\langle\sigma_0^2\rangle = 4\langle u_0^2\rangle/3r_0^2$, where $\langle u_0^2\rangle$ is the mean-square displacement, resolved along any crystal axis. However, for thermal phonons, $\langle u_T^2\rangle$ diverges logarithmically as the sample size increases, while $\sigma_T^2$ does not, and is a natural vibrational parameter for a 2D crystal.

What we emphasize is that the distribution in space of the electron density in the Wigner crystal can be characterized through the whole parameter range of magnetic field $B$, temperature $T$ and carrier density $n$ by this half-width $\lambda$. Though this can be calculated within the framework of the Einstein model, we shall in fact use the shear strain parameter $\sigma$, and model its dependence on the above parameters in the present approach. The Einstein results for $\lambda$ then can be regarded as providing one useful guideline in achieving satisfactory modelling.

### 2.1. *Modelling of the shear modulus as function of shear strain parameter*

An essential first step in setting up a model to calculate the phase diagram of the 2D Wigner crystal for a wide selection of parameter values is to relate the shear modulus $\mu$ to the dimensionless parameter $\sigma$.

As starting point, we note that Bonsall and Maradudin (1977) gave the Madelung energy of any 2D crystalline array of localized electrons. Their results were later confirmed by Borwein *et al* (1988). The ground state is a triangular crystal (one electron per lattice point on a 2D hexagonal Bravais lattice) with energy $-1.1061\, e^2/r_0$ per electron. Figure 1 displays the energies $E_1(\alpha)$ and $E_2(\alpha)$ for a simple shear strain $\alpha$ applied along the $\langle 11\bar{2}\rangle$ and $\langle 10\bar{1}\rangle$ directions, respectively. For small strains, $E_1$ and $E_2$ are close to the harmonic energy

$$E_0(\alpha) = -1.1061e^2/r_0 + \tfrac{1}{2}\mu_0\pi r_0^2\alpha^2 \tag{2.2}$$

where $\mu_0 = 0.044\, e^2/r_0^3$ is the shear modulus at $T = 0$ for a classical electron crystal. For large strains, there is both anisotropy and anharmonicity. To a very good approximation

$$E_1(\alpha) = [-1.1013 - 0.0048\cos(\sqrt{3}\pi\alpha)]e^2/r_0 \tag{2.3}$$

with $E_2(\alpha) > E_0(\alpha)$ with

$$E_1(\alpha) + E_2(\alpha) = 2E_0(\alpha). \tag{2.4}$$

The effect of this anharmonicity is to cause the shear modulus to depend on the thermal motion and zero-point motion of the electrons. We assume that this gives a Gaussian distribution† $\exp(-\alpha^2/2\sigma^2)$ of resolved shear strain along any direction with variance $\sigma^2$. Hence the mean energy for an additional infinitesimal strain $\alpha_1$ can be written as

$$\overline{E(\alpha_1)} = \int_{-\infty}^{\infty} E(\alpha + \alpha_1)\exp(-\alpha^2/2\sigma^2)\,\mathrm{d}\alpha \tag{2.5}$$

The effective shear modulus is then given by $\partial^2\bar{E}/\partial\alpha_1^2$, as $\alpha_1$ tends to zero. Substituting the expressions for $E_1$ and $E_2$ in (2.5) we obtain

$$\mu_1^*(\sigma) = \mu_1(\sigma)/\mu_0 = \exp(-D\sigma^2) \qquad \mu_2^*(\sigma) = 2 - \mu_1^*(\sigma) \tag{2.6}$$

where $D = 3\pi^2/2 = 14.8$ while $\mu_1^*$ and $\mu_2^*$ are the normalized shear moduli for simple

† In the appendix, some motivation for this assumption is provided by taking the site density $\gamma$ to move rigidly as the sites move under shear. This argument relates $\sigma$ to the half-width of the site density.

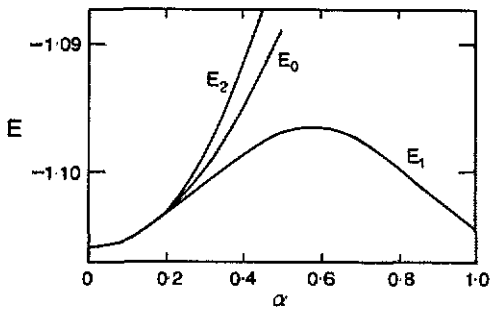


**Figure 1.** The Coulomb energy per electron, in units of $e^2/r_0$, for a 2D triangular electron crystal as a function of a static shear strain $\alpha$ parallel to the $\langle 11\bar{2}\rangle$ direction (energy $E_1$) and the $\langle 10\bar{1}\rangle$ direction (energy $E_2$). The parabola $E_0$ shows the harmonic energy variation for the zero-temperature shear modulus. The calculations were made using the expressions given by Bonsall and Maradudin (1977).

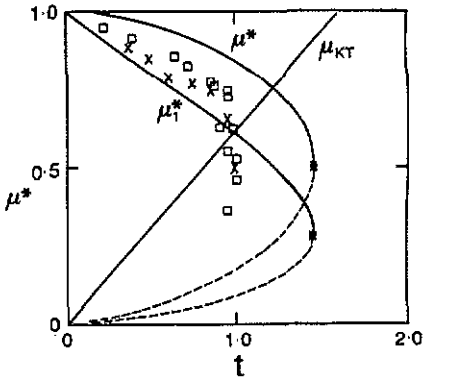


**Figure 2.** The reduced shear moduli $\mu^*$ and $\mu_1^*$, calculated from (3.2) as a function of reduced temperature $t$. The points on the lines show the anharmonic stability limit. The broken curves show the unstable solutions of (3.2). The full line $\mu_{KT}$ shows the theoretical locus of the Kosterlitz–Thouless transition. The crosses are the results from computer simulations by Morf (1979), while the squares are the experimental data of Deville *et al* (1984) for electrons on liquid helium.

shear strains along the $\langle 11\bar{2}\rangle$ and $\langle 10\bar{1}\rangle$ directions, respectively. A static shear stress on the crystal produces both types of strain and a resultant modulus $\mu^*$, isotropic by symmetry, is given by

$$1/\mu^* = 1/2\mu_1^* + 1/2\mu_2^* \qquad \mu^*(\sigma) = \mu_1^*(\sigma)\mu_2^*(\sigma). \tag{2.7}$$

The next stage is to calculate the mean-square shear produced by the propagating shear modes, angular frequency $\omega(q)$ and amplitude $U_q$, in the crystal. The mean-square component of displacement of each electron, mass $m$, along any direction is given by

$$\langle u^2\rangle = \frac{1}{2}\sum_q |U_q|^2 = \frac{1}{2}\sum_q \frac{\varepsilon}{mn\omega^2} \tag{2.8}$$

where

$$\varepsilon = (\hbar\omega_q/2)\coth(\hbar\omega_q/2k_BT) \tag{2.9}$$

is the mean energy per mode. The mean-square shear strain, resolved along any direction, is

$$\sigma^2 = \langle\alpha^2\rangle = \frac{1}{2}\sum_q q^2|U_q|^2 = \frac{1}{2}\sum_q \frac{q^2\varepsilon}{mn\omega^2} \tag{2.10}$$

for pure shear modes, and will be isotropic by symmetry in a triangular crystal with contributions from all shear modes.

## 3. Instabilities and melting

The purpose of this section is to convert the result (2.6) relating reduced shear modulus $\mu$ to half-width $\sigma$ into potentially observable predictions. First, let us consider the classical limit in zero field.

### 3.1. Classical limit

Specifically, the above calculation of the scaled shear modulus will first be employed to construct the temperature dependence of the shear modulus $\mu$ and to exhibit the instability of the lattice. A phonon model leads to a relation of the form

$$\sigma^2 = Ak_B T/\mu(\sigma) \tag{3.1}$$

$A$ being a constant and of course, model dependent.

A value of $A$ can be obtained from a simplified Debye model. An unscreened 2D plasma is incompressible in the long-wavelength limit, so we include only the shear modes (which have propagation and polarization directions in the plane of the electrons). The shear modes propagating along the two symmetry directions are: $\omega_1 = c_1 q$ where $c_1^2 = \mu_1/mn$ for $q_1$ parallel to $\langle 10\bar{1}\rangle$ and polarization along $\langle 11\bar{2}\rangle$, and $\omega_2 = c_2 q$ with $c_2^2 = \mu_2/mn$ for $q_2$ parallel to $\langle 11\bar{2}\rangle$ and polarization along $\langle 10\bar{1}\rangle$. Integrating (2.10) up to the Debye wave vector $q_D = 2/r_0$ leads to

$$\sigma^2 = (k_B T/2\pi r_0^2)(1/2\mu_1 + 1/2\mu_2) = k_B T/2\pi r_0^2 \mu = 0.0285t/\mu^*(\sigma) \tag{3.2}$$

where $t$ is the temperature normalized to the Kosterlitz–Thouless melting temperature $T_{mc} = e^2/r_0\Gamma_m k_B$, where $\Gamma_m$ has been determined experimentally to be 127 (Deville 1988) for electrons on liquid helium.

Equation (3.2) has been solved self-consistently to obtain the shear modulus $\mu^*(t)$ as a function of temperature. The results are shown, along with plots of $\mu_1^*(t)$ and $\mu^*(t)$ in figure 2. Several interesting points emerge from this admittedly simple model. First, the shear mode with $q_1$ parallel to $\langle 10\bar{1}\rangle$, which corresponds to the close-packed lines of electrons sliding past each other, softens as $t$ increases while the $q_2$ mode stiffens. It is to be noted that $\mu_1^*(t)$ decreases linearly with $t$ at low temperatures. The total shear modulus $\mu^*(t)$ also decreases to an anharmonic instability at $\mu^* = 0.5$, $t = 1.46$ and $\sigma = 0.29$. For $\sigma > 0.29$, (3.2) still has a solution (shown as a broken curve in figure 2) but the crystal will then be unstable. The Kosterlitz–Thouless transition occurs at a temperature $T_m$ such that

$$T_m = \mu a^2/4\pi k_B \tag{3.3}$$

where $a$ is the lattice spacing. This transition will therefore occur when the reduced shear modulus $\mu_{KT} = 0.62t$ as shown by the full line in figure 2. This intersects the $\mu^*(t)$ graph for this model at $t = 1.22$. Also shown in figure 2 are measurements of $\mu^*$ by Deville *et al* (1984), together with the computer simulation results of Morf (1979). The shear modulus is found to decrease linearly at low temperature and this has been shown to be due to anharmonicity in detailed calculations by Chang and Maki (1983). The rapid decrease in $\mu$ near the transition found by Morf has been ascribed to renormalization due to thermally excited dislocations.

Note that the shear modulus and the anharmonic instability in the present model can be scaled in temperature by adjusting the absolute value of $A$. Hence the relative positions of the Kosterlitz–Thouless transition and the anharmonic instability can be

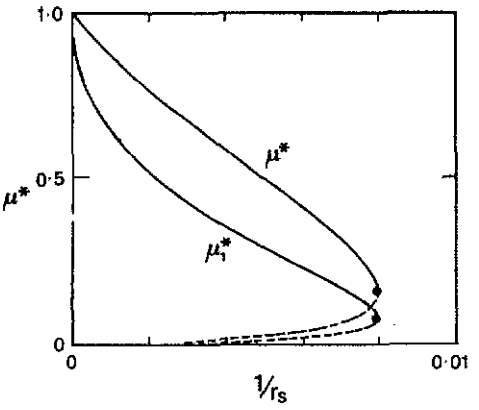


**Figure 3.** The reduced shear moduli $\mu^*$ and $\mu_1^*$, calculated from (3.4) as a function of $1/r_s$ at $T = 0$. The points on the lines show the anharmonic stability limit. The broken curves show the unstable solutions of (3.2).

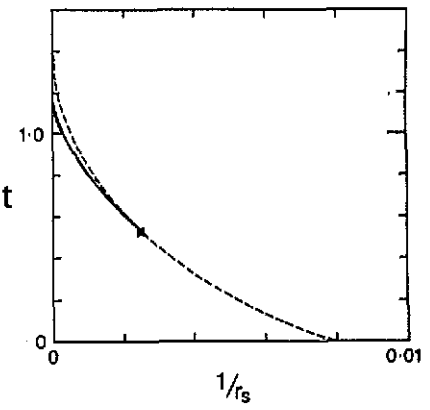


**Figure 4.** The model phase diagram of the 2D electron crystal in zero field on a $t$ versus $1/r_s$ plot. The full curve shows the locus of the Kosterlitz–Thouless transition while the broken curve is the locus of the anharmonic instability. Note the predicted change in the nature of the transition as the electron density increases.

varied and can occur very close together: with reference to figure 2 an increase in $\sigma$ by only 20% above the Debye model would bring the upper curve into accord with the available data. The two transitions are closely linked in that dislocations are produced by slip along the $\langle 11\bar{2} \rangle$ direction which corresponds to the softened $q_1$ shear mode. It is tempting to associate the region between the Kosterlitz–Thouless transition and the anharmonic instability with the postulated hexatic phase (Nelsen and Halperin 1979).

### *3.2. Quantum limit*

Equation (2.6) can also be applied to the quantum crystal at $T = 0$ in zero field. In this case $\sigma^2$ is due to zero-point shear strain and the two-mode Debye model gives

$$\sigma_0^2 = (1/3\sqrt{\pi r_s})(1/2\sqrt{\mu_1} + 1/2\sqrt{\mu_2}) = (0.45/\sqrt{r_s})(1/\sqrt{\mu_1^*} + 1/\sqrt{\mu_2^*}) \qquad (3.4)$$

where $r_s = r_0/a_B$ and $a_B = \hbar^2/me^2$ is the Bohr radius. This can be solved for $\mu^*$ and $\mu_1^*$ as functions of $1/r_s$, the results being shown in figure 3. As zero-point motion increases, the shear modulus falls until the crystal becomes unstable at $\mu^* = 0.16$ and $r_s = r_W = 125$. There are no experimental results on this transition, which is the transition Wigner originally proposed (Wigner 1934, 1938), though in two dimensions, but Ceperley has shown by computer simulation that $r_W = 33$. Hence the quantum crystal is more stable than our simple model suggests. The notorious sensitivity of $r_W$ to the model chosen is clear from the table of Care and March (1975). The Debye model probably overestimates the zero-point motion. Siringo *et al* (1991) have also shown that the force constant between disks of electronic charge is greater than for point charges. Finally this model does not consider any specifically quantum effects which may result from the overlap of the individual electronic wave functions. Nonetheless a possible mechanism for 2D Wigner quantum melting is clearly indicated, as an anharmonic instability.

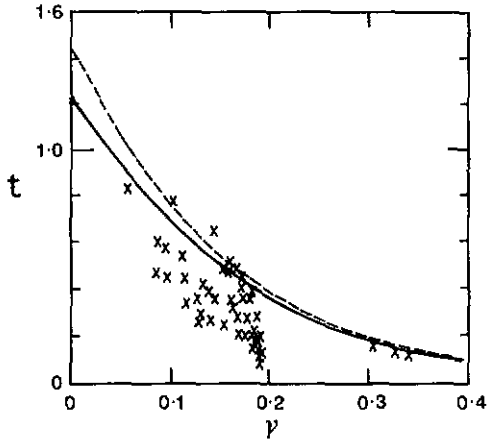


**Figure 5.** The model phase diagram of the 2D electron crystal in a magnetic field on a $t$ versus $\nu$ plot. The full curve shows the locus of the Kosterlitz–Thouless transition while the broken curve is the locus of the anharmonic instability. The data points are from Andrei *et al* (1988) and Glattli *et al* (1990).

It is interesting to follow this instability and the $K$–$T$ transition at finite temperature, as $r_s$ decreases from infinity in the classical limit, using the expression for $\sigma^2$, supplemented by thermal contributions. The loci of these transitions on the $t$–$1/r_s$ plane is shown in figure 4. At $r_s = \infty$ the $K$–$T$ transition occurs below the instability, as already discussed. But as $r_s$ decreases the two transitions merge until, for $r_s < 400$, the $K$–$T$ transition no longer occurs. In the present model the transition is an anharmonic instability for $125 < r_s < 400$.

### 3.3. *The magnetically induced Wigner solid (MIWS)*

In the quantum limit of high density, when $r_s = 0$, it is well established theoretically that an infinite magnetic field can suppress the zero-point motion and induce a classical 2D electron crystal. As the field is reduced, or as the Landau-level filling factor $\nu$ increases, the cyclotron motion of individual electrons increases with a mean-square displacement along any direction $\langle u^2 \rangle = l_B^2$, where $l_B = (\hbar/eB)^{1/2}$ is the magnetic length. If we assume that this displacement produces both longitudinal and shear strains then the resolved shear strain can be written as

$$\sigma_B^2 = 0.0285t/\mu^*(\sigma) + G\nu \tag{3.5}$$

where the first term is taken to be the same as for the classical crystal in zero field. Fourier transforming the cyclotron motion into components of longitudinal and shear displacements and integrating to find the mean-square shear strain gives $G = 0.5$ in the limit $l_B < r_0$. Taking $G = 0.5$, (3.5) is solved self-consistently. It is found that as $\nu$ increases the $K$–$T$ transition and the instability temperature decrease as shown in figure 5. For the model parameters used here, the instability lies above the $K$–$T$ transition at all fields, but the relative position could well be field dependent.

This phase diagram has some of the features of the experimental data of Andrei *et al* (1988) and Glattli *et al* (1990). However, it now seems possible that there may be regions of 2D electron liquid phases interspersed with solid phases (Jiang *et al* 1990, Buhmann *et al* 1991) and that the phase diagram calculated here could form an 'envelope' for the solid regions. On this interpretation such a liquid phase is seen in the data close to a filling factor $\nu = 0.192$. Also the three points at $\nu > 0.3$, originally excluded by

Andrei *et al* from their analysis, could represent a solid phase in this region. It is known from the zero-magnetic-field treatments of melting, already referred to above, that near $T = 0$ the phase diagram will depend sensitively on the nature of the low-lying excitations in the two phases and these are not carefully treated in the present model. It is to be noted that Lozovik *et al* (1985) have exposed an anharmonic instability as the Landau level factor increases beyond a critical value.

## 4. Discussion and summary

That there is an intimate relation between the dimensionless parameter $\sigma$ characterizing the shear strain and the electron density profile (2.1) has already been emphasized. Some work on deviations of this profile from Gaussian form is available from the study of Gann *et al* (1979). Related to this, and for the ground-state in zero magnetic field, the 3D density functional calculations of Senatore and Pastore (1990) offer a way of checking the Gaussian structure factor $\rho(k)$, by extracting the Fourier components in the periodic density in the Wigner crystal at the reciprocal lattice vectors $K_i$. Equally important would be a study of the way that shear affected the localized density profile. Underlying the present work is the model in which the 'localized Gaussian blobs' move rigidly as the lattice sites are shifted by a 'frozen phonon'. This could be tested, at least in principle, by the approach of Senatore and Pastore (1990), who refer to both BCC and FCC lattices. As pointed out by Perrin *et al* (1985), it is possible by continuous deformation via a body-centred tetragonal phase to pass from BCC to FCC; each periodic lattice could be explored to check the way in which the 'localized' blobs on the Wigner sites have to be deformed as a crystal is sheared. In connection with atomic crystals, the model of localized blobs moving without deformation is the analogue of the rigid-ion model, which in turn is equivalent to a pair force field.

Such refinements will no doubt mean that the simple modelling of $\mu$ in terms of $\sigma$ in (2.6) will have to be transcended. Nevertheless, this modelling suggests that it will be of considerable interest to explore whether Bragg reflection studies of some sort are feasible on a heterojunction. If the phonon mode found by Andrei *et al* (1988) and by Glattli *et al* (1990) is the lower hybrid magnetophonon mode derived from the shear mode, this would confirm that one is dealing with a Wigner solid; not necessarily with long-range crystalline order. So this would be the first objective of Bragg reflection studies: to demonstrate crystallinity. The second would be to test the prediction of the present study of an intimate connection between shear modulus and scattering factors.

A further point of considerable interest is to recognize that a more general theoretical model will not merely cover a range of filling factors to $\nu > 0.4$, but will need to relate Wigner crystal theory to Laughlin-like electron liquid states as well as, possibly, the Hall crystal postulated by Halperin *et al* (1986). This should then reveal what will no doubt be a close connection between the region of parameter space treated in the present work and integral and fractional quantum Hall effects. Already, a re-entrant phase diagram is emerging from experimental studies (Jiang *et al* 1990, Buhmann *et al* 1991) with a series of interspersed liquid and solid phases as $\nu$ increases. The 'envelope' of these phases seems to be close to the melting line in figure 5. The host material may also have a strong influence on the phase diagram of the 2D electrons. For instance, Kohler *et al* (1986) have suggested that a phonon-mediated transverse charge-density wave state in a quantizing magnetic field may lead to Wigner crystallization over the whole range of magnetic quantization.

Finally, to summarize, the main conclusions of the model presented here are:

(i) There are two possible instabilities: one arising directly from anharmonicity in the simple model presented; the other is a Kosterlitz–Thouless transition. As the physical parameters are varied, it is possible to find 'cross-over' between the instabilities.

(ii) The quantum limit $T = 0$ in zero field is clearly sensitive to (*a*) tunnelling, which is not incorporated in the present model; it is related to Wigner oscillator wave-function overlap and (*b*) possible ring exchange, relating to magnetism, as discussed by March and Tosi (1980).

(iii) At the present stage of development of magnetic-field-assisted Wigner crystallization, the simple model presented here seems particularly useful. The main features of the phase diagram established experimentally by Andrei *et al* (1988) and by Glattli *et al* (1990) are compatible with the present predictions of Wigner crystallization in the high-field regime, except near $T = 0$ (see figure 5) where more careful treatment of the low-lying excitations in the liquid and the crystal phases is clearly called for (for $B = 0$ see Ferraz *et al* 1978, 1979). Subsequent experiments on non-linear electrical conductivity provide further strong evidence in support of pinned Wigner crystals over a substantial range of electric field, followed eventually by 'sliding' of the Wigner crystallites.

## Appendix: Energy stored in electric field as a function of strain

The purpose of this appendix is to provide motivation from an approximate electronic theory for the phenomenological treatment of the shear modulus given in section 2.1. For convenience of presentation, we specifically treat a 3D Wigner electron crystal in zero magnetic field.

The starting point is an equilibrium crystal with localized electron densities $\gamma(r)$ centred on lattice sites $l$, the unit cell being denoted by $\Omega_l$. When shear is applied, we denote the new sites by $l + \Delta l$ and the volume of integration is through a unit cell denoted by $\Omega_{l+\Delta l}$, though the density is held constant in the shear.

If the total ground-state electron density in the crystal without shear is denoted by $\rho(r, l)$ then we assume

$$\rho(r, l) = \sum_l \gamma(|r - l|). \tag{A1}$$

Evidently, in a 'rigid blobs' model, analogous to the lattice dynamical rigid-ion model of normal metal crystals built from electrons and granular ions, the density in the sheared lattice is given by

$$\rho(r, l + \Delta l) = \sum \gamma(|r - l - \Delta l|) \tag{A2}$$

where $\Delta l$ is not necessarily constant through the unit cell. The density change $\Delta\rho(r)$ can then be written, to first-order in the (assumed small) site displacement, $\Delta l$,

$$\Delta\rho = \rho(r, l + \Delta l) - \rho(r, l) = \Delta l \cdot \text{grad}\, \rho(r, l). \tag{A3}$$

Next let us consider the energy stored in the electric field $E(r)$. By a similar argument, the change in energy per electron due to shear is approximately

$$8\pi\Delta\mathscr{E}_{\text{shear}} = \int [E^2(r, l + \Delta l) - E^2(r, l)]\, \mathrm{d}r \tag{A4}$$

where the integration is taken over the common volume of the two unit cells involved.

Writing the integrand as $(E_{l+\Delta l} + E_l)\ (E_{l+\Delta l} - E_l)$, one has again for $\Delta l$ small the approximate form $2E_l(\Delta l \cdot \text{grad}\, E)$.

At this stage we invoke Poisson's equation

$$\text{div}\, \boldsymbol{E} = 4\pi\Delta\rho \tag{A5}$$

and after some manipulation, one has for the interesting term for present purposes of $O(\Delta l^2)$, the form

$$\Delta\mathscr{E}_{\text{shear}} \sim \int E_i \Delta l \cdot (r/r)\Delta\rho\, \mathrm{d}r. \tag{A6}$$

The important conclusion here is that, when the localized density $\gamma(r) = N\exp(-r^2/\lambda^2)$, the grad $\rho$ term involved in $\Delta\rho$ contains a term of the form $\exp(-r^2/\lambda^2)2r/\lambda^2$. This is plainly the term which is strongly dependent on the half-width, $\lambda$, of the density profile; therefore in the remainder of the integrand in (A6) one use that the localized limit $\lambda$ tends to zero. Essentially then, this approximate microscopic theory provides a basis in electron theory for the phenomenological assumption embodied in (2.5) in the limit $\alpha_1 \to 0$. The argument used there is to write, for a harmonic potential $\frac{1}{2}x^2$, the result

$$\text{Energy} = (\tfrac{1}{2}x^2) \times \text{distribution in } x,$$

or for a general energy such as calculated by Bonsall and Maradudin (1977) and displayed in figure 1, $\frac{1}{2}x^2$ is replaced by $E(x)$. The distribution in $x$ written above has, in (2.5), Gaussian form with half-width $\sigma$. The above treatment therefore crucially links electron density and the shear strain dimensionless parameter, $\sigma$.

## References


Andrei E Y, Deville G, Glattli D C, Williams F I B, Paris E and Etienne B 1988 *Phys. Rev. Lett.* **60** 2765

Bhatia A B and March N H 1984 *J. Chem. Phys.* **80** 2076

Bonsall L and Maradudin A A 1977 *Phys. Rev.* B **15** 1959

Borwein D, Borwein J M, Shail R and Zucker I J 1988 *J. Phys. A: Math. Gen.* **21** 1519

Buhmann H, Joss W, van Klitzing K, Kukuskim I V, Plant A S, Martinez G, Ploog K and Timofeev V B 1991 *Phys. Rev. Lett.* **6** 926

Care C M and March N H 1975 *Adv. Phys.* **24** 101

Ceperley D M 1978 *Phys. Rev.* B **18** 3126

Chang M and Maki K 1983 *Phys. Rev.* B **18** 1646

Deville G 1988 *J. Low Temp. Phys.* **72** 135

Deville G, Valdes A, Andrei E Y and Williams F I B 1984 *Phys. Rev. Lett.* **53** 588

Durkan J, Elliott R J and March N H 1968 *Rev. Mod. Phys.* **40** 812

Elliott R J and Kleppmann W G 1975 *J. Phys. C: Solid State Phys.* **8** 2729, 2737

Ferraz, A, March N H and Suzuki M 1978 *Phys. Chem. Liquids* **8** 153; 1979 *Phys. Chem. Liquids* **9** 59

Gann R C, Chakravarty S and Chester G V 1979 *Phys. Rev.* B **20** 326

Glattli D C, Deville G, Duburcq G, Williams F I B, Paris E and Etienne B 1990 *Surf. Sci.* **229** 334

Halperin B I, Tesanovic Z and Axel F 1986 *Phys. Rev. Lett.* **57** 922

Jiang H W, Willett R L, Stormer H L, Tsui D C, Pfeiffer L N and West K W 1990 *Phys. Rev. Lett.* **65** 633

Johnson R A 1988 *Phys. Rev.* B **37** 3924

Kohler H, Roos M and Dato P 1986 *J. Phys. C: Solid State Phys.* **19** 5215

Kosterlitz J M and Thouless D J 1973 *J. Phys. C: Solid State Phys.* **6** 1181; 1978 *Prog. Low Temp. Phys.* B **7** 371

Lea M J and March N H 1990 *Phys. Chem. Liq.* **21** 183

Lozovik Yu E, Fartztdinov V M and Abdullaev B 1985 *J. Phys. C: Solid State Phys.* **18** L807

March N H 1989 *Phys. Rev.* B **40** 3356; 1988 *Phys. Rev.* A **37** 4526

March N H and Tosi M P 1985 *J. Phys.* A **18** L643

March N H and Tosi M P 1980 *Phys. Chem. Liquids* **10** 113
Morf R H 1979 *Phys. Rev. Lett.* **43** 931
Nagara H, Nagata Y and Nakamura T 1987 *Phys. Rev.* A **36** 1859
Nelson D R and Halperin B I 1979 *Phys. Rev.* B **19** 2457
Perrin R C, March N H and Taylor R 1985 *Solid State Commun.* **53** 287
Ploog K 1990 *Physica* B + C at press
Saitoh M 1988 *Surf. Sci.* **196** 8
Senatore G and Pastore G 1990 *Phys. Rev. Lett.* **64** 303
Siringo F, Lea M J and March N H 1991 *Phys. Chem. Liquids* at press
Wigner E P 1934 *Phys. Rev.* **46** 1002; 1938 *Trans. Faraday Soc.* **34** 678